Structural and Spectroscopic Studies of a Nanostructured Silicon – Perovskite Interface

Roberto Gonzalez-Rodriguez[a], Viviana C.P. Costa,[a] Géraud Delport,[b] Kyle Frohna,[b] Robert L. Z. Hoye,[c] Samuel D. Stranks,[b] and Jeffery L. Coffer[a*]

While extensively investigated in thin film form for energy materials applications, this work investigates the formation of $APbBr_3$ structures (A = $CH_3NH_3^+$ (MA), Cs^+) in silicon and oxidized silicon nanotubes (SiNTs) with varying inner diameter. We carefully control the extent of oxidation of the nanotube host and correlate the relative Si / Si oxide content in a given nanotube host with the photoluminescence quantum efficiency (PLQE) of the perovskite. Complementing these measurements is an evaluation of average PL lifetimes of a given $APbBr_3$ nanostructure, as evaluated by time-resolved confocal photoluminescence measurements. Increasing Si (decreasing oxide) content in the nanotube host results in a sensitive reduction of $MAPbBr_3$ PLQE, with a concomitant decrease in average lifetime (τ_{ave}). We interpret these observations in terms of decreased defect passivation by a lower concentration of oxide species surrounding the perovskite. In addition, we show that the use of selected nanotube templates leads to more stable perovskite PL in air over time (weeks). Taken in concert, such fundamental observations have implications for interfacial carrier interactions in tandem Si/perovskite photovoltaics.

Introduction

Investigations of the fundamental properties of perovskites continue at a frantic pace, coupled with dedicated efforts in potential commercialization directed toward applications in light emitting diodes (LEDs),[1-11] lasing,[12-16] photodetectors,[17-20] and most notably, photovoltaics.[21-26] These materials have the general structure ABX_3, where A is an organic/inorganic cation (e.g. methylammonium (MA), formamidinium (FA), cesium (Cs)), B is a metal cation (e.g. Pb^{2+}, Sn^{2+}) and X is a halide anion (e.g. Cl^-, Br^-, I^-). The optical and electronic properties of a given perovskite most sensitively depend on the ABX_3 composition and domain size.[27]

The most promising photovoltaic designs to date employ a tandem silicon / perovskite configuration, reaching efficiency values now at 28%.[25] Nevertheless, a fundamental understanding of interfacial charge carrier recombination between perovskite and silicon components is lacking, especially as layer thicknesses diminish and the two semiconducting moieties come into closer proximity. To interrogate such interactions in the absence of an active recombination layer, we evaluate here the interaction of perovskites with elemental Si based on $APbBr_3$ (A= MA or Cs) formed within the interior of hollow silicon nanotubes of well-defined morphology and composition (Figure 1), using photoluminescence (PL) as an experimental probe. Perovskites such as $MAPbBr_3$ possess a number of ideal properties in this regard: a direct bandgap (E_g ~2.3 eV) and associated strong luminescence (~530 nm) with significant quantum efficiency, along with a relatively facile processability.[28]

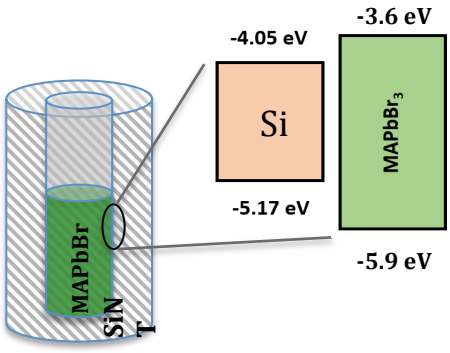

Figure 1. Illustration of a $MAPbBr_3$ perovskite formed within the interior of a Si NT, and the corresponding approximate band level energetics (neglecting interfacial effects). Si values are taken from ref. 29, those for $MAPbBr_3$, ref. 30 .

[a.] *Department of Chemistry and Biochemistry, Texas Christian University, TCU Box 298860, Fort Worth, Texas 76129, USA.*
[b.] *Cavendish Laboratory, University of Cambridge, JJ Thompson Avenue, Cambridge CB3 0HE, UK.*
[c.] *Department of Materials Science and Metallurgy, University of Cambridge, 27 Charles Babbage Road, Cambridge CB 3 0FS, UK.*

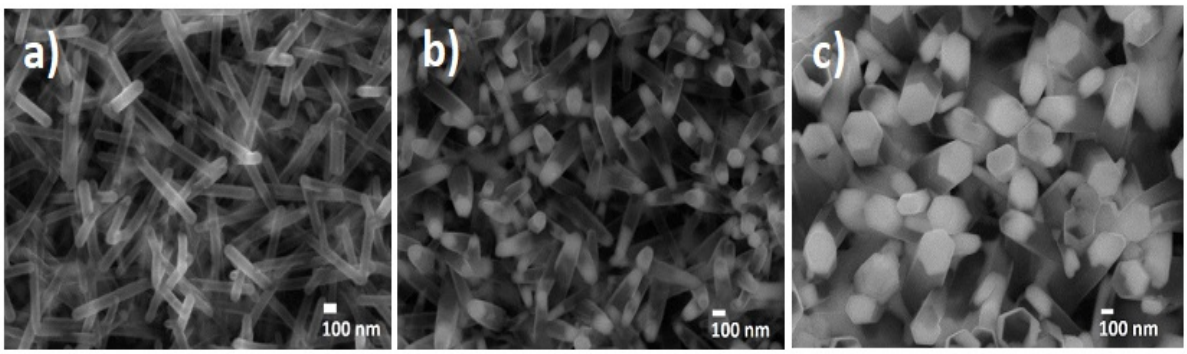

Figure 2. SEM of Si NTs loaded with $MAPbBr_3$, a) 30 nm ID Si NTs, b) 70 nm ID Si NTs and c) 200 nm ID Si NTs.

An additional consideration is the potential stability of a given perovskite structure and morphological control (during its fabrication) provided by structurally well-defined porous templates such as these SiNTs. The decomposition of perovskites can be catalyzed by moisture,[31] applied voltage,[32] light, [33] and high temperatures, [33] all of which can seriously affect their operational stability. The stability of perovskites can be improved with the addition of surface passivating protecting layers[34] or by perovskite encapsulation in porous materials to avoid environmental degradation, as reported in the use of alumina,[35] mesoporous titanium oxide,[36] porous GaN,[37] porous silica[38] and silicon nanotubes (SiNTs) [39-41] for this purpose. SiNTs are an appealing option, as they provide sensitive size tunability in terms of inner diameter, Si shell thickness, as well as nanotube length, along with the fact the associated fabrication process of this material is compatible with current semiconductor industry manufacturing processes.

In this paper we describe the formation of $APbBr_3$ nanostructures in Si and oxidized (SiO_2) NTs as templates of varying inner diameter. We carefully control the extent of oxidation of the nanotube host and correlate the relative Si content in a given nanotube host with the PL quantum efficiency of the perovskite. Complementing these measurements is an evaluation of average PL lifetimes of a given $MAPbBr_3$ nanostructure, as evaluated by confocal PL decay measurements. It is found that the PLQE clearly increases with decreasing Si / increasing oxide content, with an associated lengthening of average PL lifetime. We also see an improvement in stability of the steady state PL intensity as a function of storage time in air for selected nanotube templates (relative to non-stabilized bulk films).

Results and discussion

Using a silicon nanotube fabrication process previously established by our group,[42] we selected three different inner nanotube diameters (ID) for perovskite incorporation: 30, 70, and 200 nm ID Si NTs, with TEM images of these structures shown in Supporting Information (Supp Info) Figure S1. A straightforward precursor infiltration procedure, followed by removal of excess reagents and mild annealing (90 ^oC, 30 min), is used to achieve the formation of $MAPbBr_3$ (for example) within a given SiNT, with a number of complementary experimental methods (SEM, TEM, as well as EDX point and linescans for each) confirming successful perovskite encapsulation. In Figure 2, SEM images of 30, 70 and 200 nm ID Si NTs loaded with $MAPbBr_3$ are shown, with the perovskite nanostructures visibly evident at the nanotube tips; corresponding TEM images are shown in Supp Info Figure S2. Associated energy dispersive X-ray (EDX) measurements (Table S1) are consistent with the theoretical stoichiometric 1:3 ratio for Pb:Br, and EDX line scans (Figure 3, 70 nm ID SiNTs infiltrated with $MAPbBr_3$; others in Supp Info Fig S3) are consistent with the $MAPbBr_3$ nanostructures being confined within the tube.

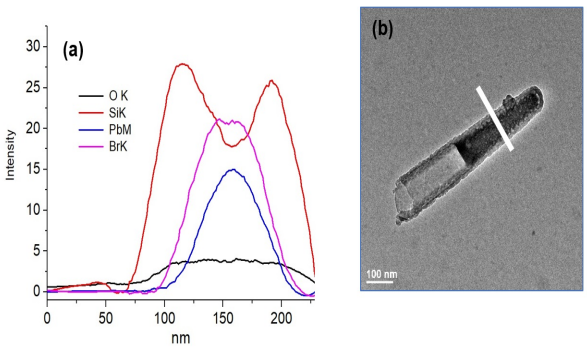

Figure 3. (a) EDX linescan and (b) associated TEM image of 70 nm ID Si NTs infiltrated with $MAPbBr_3$.

Finally, X-ray powder diffraction (XRD) measurements of these $MAPbBr_3$/SiNT films confirm the presence of the perovskite in the cubic phase, with requisite reflections (and relative intensities) clearly evident (Supp info Figure S4) and consistent with the literature.[43] Selected d-spacing values are also observable by high resolution (HR) TEM; Lattice spacings for $MAPbBr_3$ in 70 nm ID Si NTs, with d = 0.410 nm and d = 0.290, consistent with (110) and (200) orientations, respectively, can be

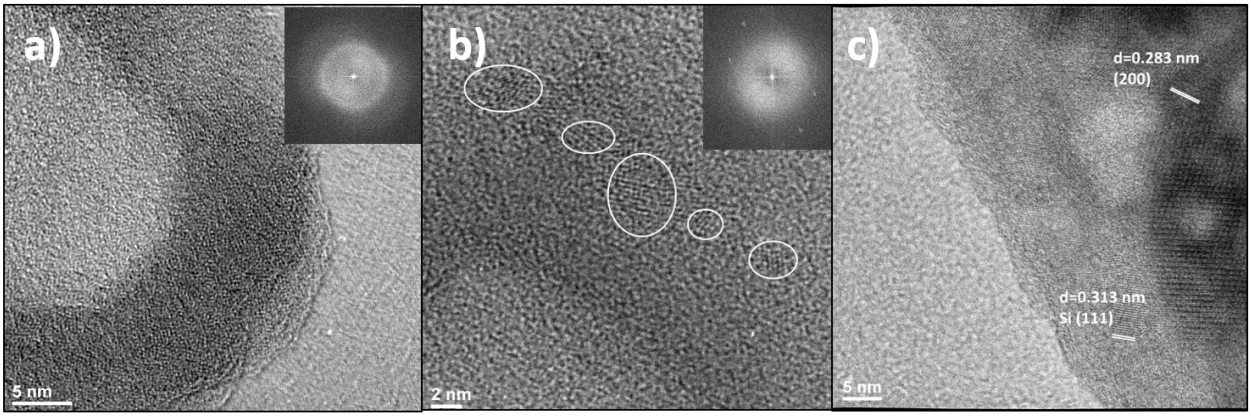

Figure 4. TEM images of (a) as-prepared 30 nm ID SiNTs; (b) partially-oxidized (600oC, 6 hrs) 30 nm ID SiNTs, with crystalline Si domains circled; (c) thermally-annealed 30 nm ID SiNTs (700 oC, 2 hrs, inert atmosphere). For (a) and (b), insets containing the FFTs associated with a given image are included.

observed in high resolution TEM (Supp Info Figure S5). Importantly, the interfacial boundary between the perovskite and SiNT host can be visualized in these images.

Prior to perovskite infiltration/formation, 70 nm ID Si NTs were oxidized in air at high temperature (600 ^oC) under carefully-controlled durations (3 or 6 hrs) to obtain different ratios of O:Si (at %) ranging from 0.4 to 2.3 (EDX-TEM, Table S1). Selected SiNTs of 30 and 200 nm inner diameter were also transformed immediately/completely to fully oxidized material (SiO_2) by annealing at 700 ^oC for 7 hrs (herein referred to as 'SiO_2/perov'). Irrespective of template, these oxidative processes did not change the initial nanotube morphology (Supporting Info Figure S3). However, from a microstructural perspective, the as-formed Si shell appears amorphous, as gauged by a lack of observed lattice spacings in high resolution TEM imaging (Figure 4a) and an associated Raman spectrum for this type of sample with a broad feature near 490 cm^{-1} (Supp Info Figure S6), consistent with amorphous Si (a-Si).[44] After intensive annealing in oxygen for several hours at >650 ^oC, nanocrystalline Si domains are observable in the nanotube shell (Figure 4b). While the as-formed Si NTs expose an amorphous character, we can also create well-defined crystalline Si – perovskite interfaces by annealing a nanotube sample in an inert atmosphere, followed by $MAPbBr_3$ precursor infiltration and perovskite formation (Figure 3c); lattice spacings associated with both crystalline Si as well as perovskite are readily observed, and the Raman spectrum sharpens considerably with a shift to a maximum near 518 cm^{-1} (classic signature for crystalline Si) [44] (Supp Info Figure S6).

In terms of photophysical properties, typical UV-visible absorption and PL spectra, along with a confocal PL image, of 70 nm ID SiO_2 NTs loaded with $MAPbBr_3$ (herein referred to as perov/SiO_2) are shown in Figure 5. The band gap of this type of perovskite nanostructure was estimated from an

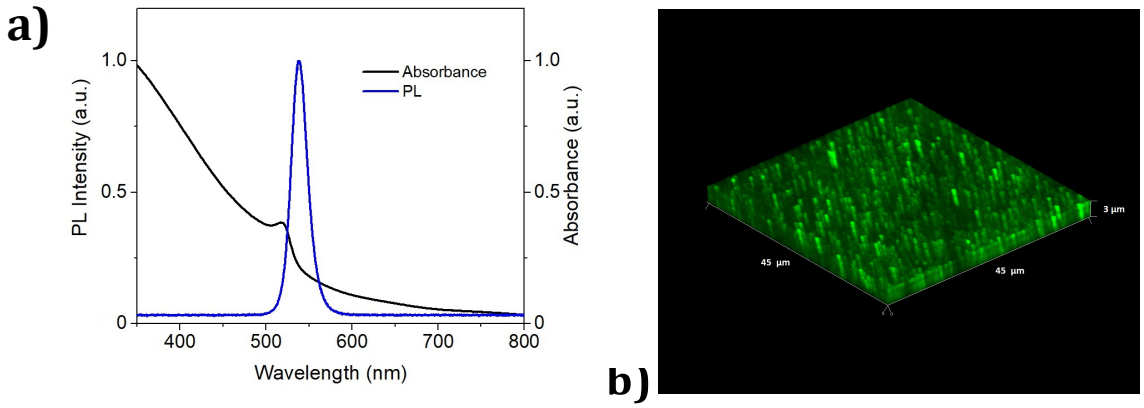

Figure 5. 70 nm ID SiO_2 NTs loaded with $MAPbBr_3$: a) Normalized absorption and PL spectra (λ_{ex} = 370 nm) and b) Confocal PL image of 70 nm ID SiO_2 NTs loaded with $MAPbBr_3$. (λ_{ex} = 458 nm; 45 µm x 45 µm area)

analysis of the onset of absorption or PL maximum (Supp Info Figure S7b) show a value of 2.3 eV for SiO_2/perov formed within 30, 70 and 200 nm ID NTs, in agreement with values reported previously for $MAPbBr_3$ in silica.[45] In the case of $MAPbBr_3$ templated by 30, 70, and 200 nm ID SiNTs (herein referred to as perov/Si), a slightly smaller bandgap is found (2-2.1 eV) (Supp info Figure S7a-b). Normalized PL spectra for 30, 70, 200 nm ID perov/SiO_2 & perov/Si are shown in Supporting Info Figure S7, with an emission maximum observed for all samples at 533 ± 3 nm. Using confocal PL imaging of the perov/Si formed within the 70 nm ID NTs (as well as 200 nm ID NTs), it is possible to observe the wire-like morphology of the emissive perovskite species (Figure 4b; Supporting info Figure S8).

Using an established integrating sphere technique[46] PL quantum efficiency (PLQE) was evaluated for $MAPbBr_3$ housed within 70 nm ID nanotubes with different amounts of Si, tuned by careful oxidation of the as-formed SiNT films. Importantly, a plot of perovskite PLQE versus Si content (expressed as the ratio O:Si, varied from 0.4 to 2.3) for a fixed nanotube diameter reveals a linear increase in PLQE with decreasing amount of Si / increasing oxide content (Figure 6).

There are three possible factors to consider in interpreting this relationship: 1) increased oxide passivation of defects or wider bandgap material in the perovskite phase,[47-50] resulting in an enhanced PL QE; 2) charge transfer quenching of photo-excited charge carriers in the perovskite at the interface with the silicon, resulting in a reduction in PL QE; 3) non-radiative energy transfer from the $MAPbBr_3$ to the Si nanocrystals.[51,52] The relationship between composition of the nanotube template and perovskite PL QE can be interpreted in terms of a Perrin-type static quenching model,[53] where the total volume of the quenching species can be viewed as an ensemble of interfacial defects (perhaps induced by elemental Si nanocrystals present in the cylindrical sheath of silicon oxide; i.e. the higher concentration of Si NCs, the lower the $MAPbBr_3$ PL QE). Thus from this perspective the greater concentration of oxide at a given interface, the stronger the intrinsic emission associated with the $MAPbBr_3$.

While one could propose Auger-like quenching processes[54] for $MAPbBr_3$ based on an interaction of perovskite carriers with Si carriers photogenerated in the Si nanostructures, or some type of energy transfer contribution between perovskite and elemental Si, the dominant role of free carriers and associated coulombic interactions in $MAPbBr_3$ photophysics likely reduces these contributions relative to an oxide passivation mechanism

There is a wide variety of PLQE values reported in the literature for $MAPbBr_3$ in general and this material formed within mesoporous silica in particular.[43,45] These values range from ~2% for $MAPbBr_3$ films[43] to values >50% for $MAPBr_3$ and $CsPbBr_3$ in very small diameter silica.[45] We do observe a

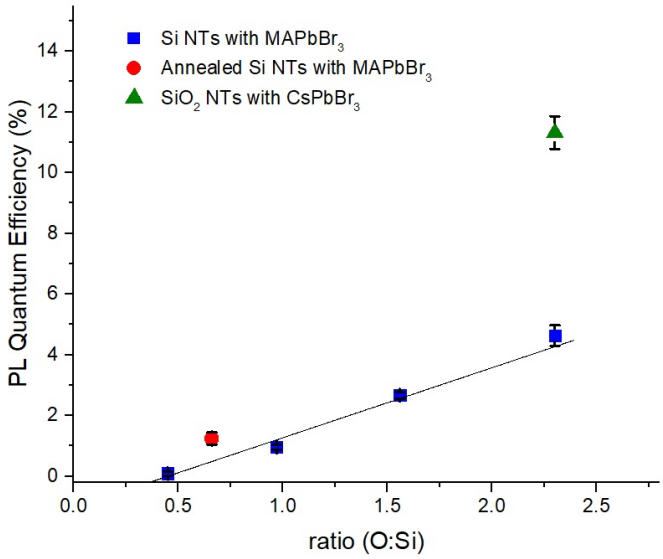

Figure 6. a) PLQE for $MAPbBr_3$ loaded into thermally oxidized 70 nm ID SiNTs as a function of increasing oxide content. All samples were exposed to a modest vacuum (ca. 10^{-2} torr) at room temperature for 10-12 hrs immediately prior to PLQE measurements. λ_{ex} = 405 nm at ~30 mJ/cm².

	Composition PL lifetime (ns)	
NT Inner diameter	perov /Si	perov/SiO_2
30 nm	5 ± 3	3 ± 1
70 nm	4 ± 1	8 ± 3

Table 1. Average PL lifetime range (ns) for formed within a given nanotube framework. Lifetime is defined here as the time taken to fall to 1/e of the initial intensity.

significant boost in perovskite PL QE when we replace methylammonium with cesium, as in the case of $CsPbBr_3$ housed within 70 nm ID SiO_2 NTs, with a corresponding QE of ~11.3 % (Figure 6). While our samples here are treated with a modest vacuum prior to QE measurements, it is noted that our perovskite precursor infiltration into SiNT structures occurs in ambient air and not in a controlled environment. We note that the PLQE values here are external values as measured and do not take into account the outcoupling efficiency of photons from the structures;[55] given we are not significantly changing the diameter of the tube and hence optical properties as we change the O:Si ratio at the interface, we do not expect the trends to be influenced by any outcoupling changes.

To complement the above PLQE measurements, confocal time-resolved (TR) PL microscopy mapping was performed on the $MAPbBr_3$ / nanotube platforms. In Figure 7 we compare the samples corresponding to 70 nm NT, either made of Si (Figure 7a and d) or SiO_2 (Figure 7b and e). We see that they both present a large spatial heterogeneity in PL intensity and PL lifetimes. We show the distribution of intensity and lifetimes in Figures 7c and f, respectively. We see that the PL lifetimes

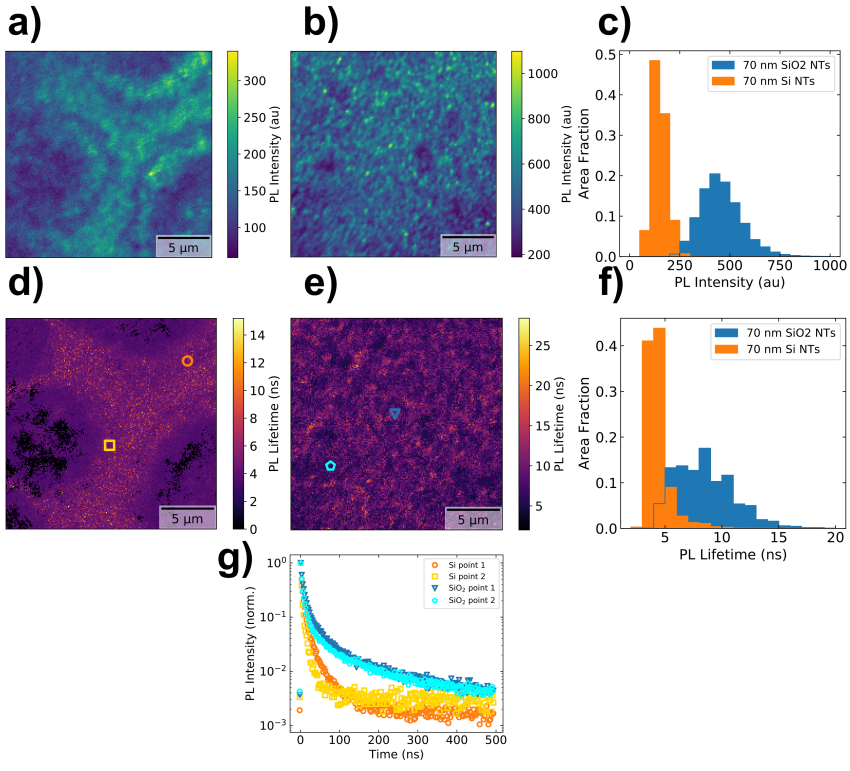

Figure 7. a) PL intensity map for perov/Si housed within 70 nm ID NTs. b) PL intensity map for perov/SiO_2 housed within 70 nm ID NTs. c) Histogram of PL intensities extracted from maps shown in panels a and b. d) PL lifetime map for $MAPbBr_3$ housed within 70 nm ID Si NT film. e) PL lifetime map of perov/SiO_2 housed within 70 nm ID NTs. f) Histogram of PL lifetimes extracted from maps shown in panel d and e. PL lifetime is defined here as the time taken to fall to 1/e of the initial intensity. g) PL lifetime decay curves extracted from the points marked in panels d) and e). Measurements were performed with pulsed 405-nm excitation (2 MHz repetition rate, 0.4 mJ/cm^2 fluence).

(Figure 7f) for the Si sample range between 0 and 5 ns, while the lifetimes for the SiO_2 sample are significantly larger, with values between 5 and 15 ns. Additionally, we see that the PL intensities (Figure 7c) are globally larger for the SiO_2 than the Si one, with values ranging between 500 and 1000 counts instead of 100-300 counts. Therefore, we see that the change between SiO_2 and Si and clearly induces a quenching of the PL, affecting both the PL intensities and lifetimes. We show lifetime decays from representative points in the Si and SiO_2 based NT samples in Figure 7g. All of the samples show a large fast decay in the early times and this dominates the values shown in the lifetime maps. However, the SiO_2 based samples show a larger contribution from a long lived decay at the longer times, whereas this is not observed in the Si based nanotubes. As seen in Supp Info Figure S10, we also observe a decrease of the PL lifetimes when the diameter of the SiO_2 NT decreases from 70 to 30 nm, with lifetime values decreasing from 8 ns (70 nm) to to 3 ns (30 nm). These microscopic results confirm the previous discussion and the interpretation of the PLQE values above; furthermore, such changes in average lifetime are consistent with a relative increase in fraction of non-radiative recombination due to charge carrier confinement within the nanotube dimensions.

Finally we address the impact of nanotube template identity on observed stability of $MAPbBr_3$ PL as a function of time. For a given template, along with a bulk film composed of micro-sized $MAPbBr_3$ cubes, we track the normalized changes in perovskite emission intensity using a PL microscope for samples ranging from freshly-prepared to 35 days old (with storage between measurements in a desiccator). From an analysis of the data (Figure 8), it is clear that $MAPbBr_3$ formed within a 70 nm ID nanotube is stabilized most effectively over a 35 day period (retaining ca 90% emission for SiO_2; 70% for Si) compared to the bulk, non-templated control (~40% PL remaining). Another point of emphasis is the significantly smaller standard deviations observed for nanotube-templated perovskite emission measurements relative to the large values for the bulk, which degrades in a rather heterogeneous manner (i.e. uniform emission for the former, and bright spots dispersed across mostly dark regions for the latter). Within the nanotube template samples, it is also clear that the 70 nm ID nanotube is superior with regard to stability to the 30 nm and 200 nm inner diameter nanotubes, similar to that observed previously for the mixed $MAPbI_{1-x}Br_x$ class of perovskites formed

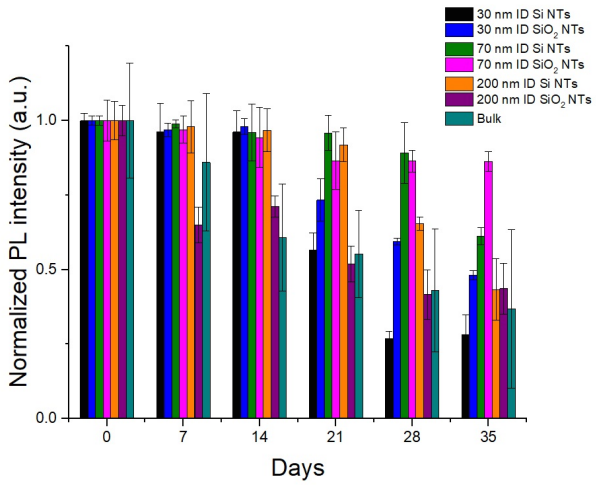

Figure 8. Changes in normalized emission intensity for $MAPbBr_3$ formed within various silicon nanotube templates as a function of time. Data for a bulk film composed of micro-sized $MAPbBr_3$ cubes is also included for control purposes.

within SiNTs of varying diameter.[41] Such a trend is presumably related to a structural 'sweet spot' for exposure of the perovskite to the surroundings. Of the three SiNT inner diameters employed in these experiments, the 200 nm value templates formation of a perovskite that acts structurally bulk-like (that is, for $MAPbI_3$, a typical tetragonal to orthorhombic phase transition occurs at 110K). This is not the case for the 70 nm ID SiNT, where the phase transition is suppressed in the resultant perovskite that is formed.[40] For the smallest Si NT template (30 nm ID), capillary forces interfere with efficient filling of a given nanotube with perovskite precursor, resulting in even smaller perovskite nanostructure domains with greater surface areas and, given the porous sidewalls, exposure to deleterious moisture, oxygen, etc.[41] Thus this structure is significantly less stable than the 70 nm one. In general, we propose that the greater retention of PL intensity for $MAPbBr_3$ formed within a given nanotube is a reflection of the ability of these Si-containing nanoscale platforms to stabilize the perovskite against moisture and environmental degradation.

Conclusions

Taken in concert, these experiments establish a clear correlation between interfacial Si/oxide content and (encapsulated) perovskite PLQE; the longer average PL lifetimes for the perovskite housed in oxidized Si NT interfaces ('perov/SiO_2') relative to the Si rich nanotube ('perov/Si') evaluated via confocal PL microscopy are consistent with these PLQE measurements. While it is not yet possible to cleanly decouple the role of oxide passivation from Si carrier-induced quenching of perovskite PL, this sensitive influence of nanotube composition on perovskite photophysics and associated stability affirms the utility of such relatively well-defined SiNT constructs to house and direct the properties of encapsulated semiconductors such as these of the $APbX_3$ family. Further investigations of the properties and utility of more complex compositions, including mixed cationic A sites as well as halide species, are underway.

Experimental methods

Materials and Instrumentation. Lead Bromide ($PbBr_2$), Zinc Nitrate ($Zn(NO_3)_2$), and Hexamethylenetetramine (HTMA) were purchased from Sigma-Aldrich. Methyl ammonium bromide (MABr) was purchased from Great Solar. Morphological characterization was done with field emission scanning electron microscopy (FESEM) using a JEOL-JSM-7100F operating at 15 kV with an energy-dispersive X-ray (EDX) detector; Transmission electron microscopy (TEM), using a JEOL JEM-2100 operating at 200 kV. Absorption spectra were recorded using a Cary 60 spectrophotometer; PL properties were measured with a Nikon Optiphot Fluorescence microscope with a 100W Hg lamp and excitation filter centered at 370 nm and interfaced to an Ocean Optics spectrometer with 2048-element linear CCD-array detector. PL quantum efficiency was measured with an integrated sphere from Newport using a laser excitation wavelength of 405 nm at 18 mW cm^{-2}. Selected confocal imaging was carried out at TCU using a Zeiss LSM710 laser scanning confocal microscope with a laser excitation wavelength of 458 nm (15 mW). Confocal time resolved photoluminescence images and single decays were measured using a confocal microscope setup (PicoQuant, MicroTime 200). The excitation laser was a 405 nm pulsed diode (PDL 828-S"SEPIA II", PicoQuant, pulse width of ~100 ps) was directly focused onto the perovskite surface with an air objective (100x, 0.9 NA). The photoluminescence signal was separated from the excitation light (405 nm) using a dichroic mirror (Z405RDC, Chroma). The PL response was then focused onto a SPAD detector for the single photon counting (time resolution of 100 ps) through a pinhole (50 μm), with an additional 410 nm longpass filter. Laser repetition rates of 2 MHz were used for the PL maps, with a 0.4 mJ/cm^2 fluence.

Silicon / Silicon oxide nanotube fabrication. ZnO nanowire templates were growth on a previously treated substrate (FTO glass, Silicon wafer, Quartz glass slide) with ZnO nanocrystal seeds.[42] These substrates were immersed in a solution containing $Zn(NO_3)_2$ and HTMA. As Si NTs inner diameter is dictated by the ZnO NW diameter, in order to obtain 30 nm and 70 nm diameter nanowires, the concentration of $Zn(NO_3)_2$ and HTMA was 0.005 M and 0.02 M, respectively, for 3 hrs duration at 95 °C. For the formation of 200 nm diameter ZnO NWs, a concentration of 0.1 M was used for 9 hrs at 95 °C. Silicon deposition was achieved on these ZnO nanowire-containing substrates by the exposure of a given ZnO NW/substrate sample in a quartz tube at 530 °C for 5 min to a dilute (0.5%) SiH_4 in Helium. Finally, in another quartz reactor, this Si-coated / ZnO sample was exposed to vapor from heated ammonium chloride at 500 °C for 2 hr was used to etch the ZnO core, yielding a final product of Si nanotubes. Silicon oxide (SiO_2) nanotubes were obtained by oxidation of silicon nanotubes, achieved by heating a given SiNT sample in a quartz tube in an oxygen atmosphere at 700 °C for 6 hr.

Perovskite loading / formation. In a manner similar to our previously published procedure,[39-41] silicon/silicon oxide nanotubes were soaked for 2 hr at 60 °C in a solution containing a 1:1 mol ratio of MABr (or CsBr) and $PbBr_2$ in DMF at a concentration of 200 mM. The samples were then spun at 7000 rpm for 40 s (to remove excess reactant solution), and finally the sample was baked for 30 min at 95 °C.

Conflicts of interest

There are no conflicts to declare.

Acknowledgements

This work was supported by the Robert A. Welch Foundation (Grant P-1212 to JLC). This project has also received funding from the European Research Council (ERC) under the European Union's Horizon 2020 research and innovation programme (grant agreement number 756962). S. D. S. acknowledges support from the Royal Society and Tata Group (UF150033). GD would like to acknowledge to Royal Society for funding through a Newton International Fellowship. K.F. acknowledges a George and Lilian Schiff Studentship, Winton Studentship, the Engineering and Physical Sciences Research Council (EPSRC) studentship, Cambridge Trust Scholarship, and Robert Gardiner Scholarship. R.L.Z. H. acknowledges funding from the Royal Academy of Engineering under the Research Fellowships scheme (No.: RF\201718\17101).

Notes and references

1. B. Zhao, S. Bai, V. Kim, R. Lamboll, R. Shivanna, F. Auras, J. Richter, L. Yang, L. Dai, M. Alsari, X.-J. She, L. Liang, J. Zhang, S. Lilliu, P. Gao, H. Snaith, J. Wang, N. Greenham, R. Friend, D. Du. *Nature Photonics,* **2018**, *12*, 783-789

2. Q. Zhang, M. Tavakoli, L. Gu, D. Zhang, L. Tang, Y. Gao, J. Guo; Y. Lin, S.-F. Leung, S. Poddar, Y. Fu, Z. Fan. *Nature Communications,* **2019,** *10* (1), 727.

3. S. Veldhuis, P. Boix, N. Yantara, M. Li, T. Sum, N. Mathews, S. Mhaisalkar, *Adv. Mater*. **2016**, 28, 6804–6834.

4. Y.-H. Kim, H. Cho, T.-W. Lee. *Proc. Natl. Acad. Sci. U.S.A.* **2016**, 113, 11694–11702.

5. B. Sutherland, E. Sargent. *Nat. Photonics.* **2016**, 10, 295–302.

6. Y.-H. Kim, H. Cho, J. Heo, T.-S. Kim, N. Myoung, C.-L. Lee, S. Im, T.-W. Lee. *Adv. Mater*. **2015**, 27, 1248–1254.

7. Z. Xiao, R. Kerner, L. Zhao, N. Tran, K. Lee, T.-W. Koh, G. Scholes, B. Rand. *Nat. Photonics*. **2017**, 11, 108–115.

8. Z.-K. Tan, R. Moghaddam, M. Lai, P. Docampo, R. Higler, F. Deschler, M. Price, A. Sadhanala, L. Pazos, D. Credgington, et al. *Nat. Nanotechnol*. **2014**, 9, 687–692.

9. H. Cho, S.-H. Jeong, M.-H. Park, Y.-H. Kim, C. Wolf, C.-L. Lee, J. Heo, A. Sadhanala, N. Myoung, S. Yoo, S. Im, R. Friend, T.-W. Lee. *Science* **2015,** *350*, 1222.

10. M. Yuan, L. Quan, R. Comin, G. Walters, R. Sabatini, O. Voznyy, S. Hoogland, Y. Zhao, E. Beauregard, P. Kanjanaboos, Z. Lu, D. Kim, E. Sargent. *Nature Nanotechnology.* **2016,** *11*, 872

11. N. Wang, L. Cheng, R. Ge, S. Zhang, Y. Miao, W. Zou, C. Yi, Y. Sun, Y. Cao, R. Yang, Y. Wei, Q. Guo, Y. Ke, M. Yu, Y. Jin, Y. Liu, Q. Ding, D. Di, L. Yang, G. Xing, H. Tian, C. Jin, F. Gao, R. Friend, J. Wang, W. Huang. *Nature Photonics.* **2016,** *10*, 699.

12. F. Deschler, M. Price, S. Pathak, L. Klintberg, D.-D. Jarausch, R. Higler, S. Hüttner, T. Leijtens, S. Stranks, H. Snaith, M. Atatüre, R. Phillips, R. Friend, *The Journal of Physical Chemistry Letters.* **2014,** *5* (8), 1421-1426.

13. G. Xing, N. Mathews, S. Lim, N. Yantara, X. Liu, D. Sabba, M. Grätzel, S. Mhaisalkar, T. Sum. *Nature Materials.* **2014,** *13*, 476

14. H. Zhu, Y. Fu, F. Meng, X. Wu, Z. Gong, Q. Ding, M. Gustafsson, M. Trinh, S. Jin, X.-Y. Zhu. *Nat. Mater*. **2015**, 14, 636–642.

15. P. Cegielski, A. Giesecke, S. Neutzner, C. Porschatis, M. Gandini, D. Schall, C. Perini, J. Bolten, S. Suckow, S. Kataria, B. Chmielak, T. Wahlbrink, A. Petrozza, M. Lemme. *Nano Letters.* **2018,** *18* (11), 6915-6923.

16. Z. Li, J. Moon, A. Gharajeh, R. Haroldson, R. Hawkins, W. Hu, A. Zakhidov, Q. Gu, *ACS Nano.* **2018,** *12* (11), 10968-10976.

17. L. Dou, et al. *Nat. Commun*. **2014***, 5*, 5404.

18. Y. Fang, Q. Dong, Y. Shao, Y. Yuan, J. Huang. *Nat. Photon.,* **2015***, 9*, 679–686 .

19. M. Zhang, F. Zhang, Y. Wang, L. Zhu, Y. Hu, Z. Lou, Y. Hou, F. Teng. *Scientific Reports.* **2018,** *8* (1), 11157.

20. D. Chun, Y. Choi, Y. In, J. Nam, Y. Choi, S. Yun, W. Kim, D. Choi, D. Kim, H. Shin, J. Cho, J. Park. *ACS Nano.* **2018,** *12* (8), 8564-8571.

21. W. Yang, B.-W. Park, E. Jung, N. Jeon, Y. Kim, D. Lee, S. Shin, J. Seo, E. Kim, J. Noh, et al. *Science*. **2017**, 356, 1376–1379.

22. J.-P. Correa-Baena, A. Abate, M. Saliba, W. Tress, T. Jesper Jacobsson, M. Graẗzel, A. Hagfeldt. *Energy Environ. Sci*. **2017**, 10, 710–727.
23. N. Aeineh, E. Barea, A. Behjat, N. Sharifi, I. Mora-Sero. *ACS Appl. Mater. Interfaces.* **2017**, 9, 13181–13187.
24. S. Stranks, H. Snaith, *Nat. Nanotechnol*. **2015**, 10, 391–402.
25. A. Extance. *Nature*, **2019**, 570, 429-432.
26. J.-P. Correa-Baena, M. Saliba, T. Buonassisi, M. Grätzel, A. Abate, W. Tress, A. Hagfeldt. *Science*. **2015**, 358, 739-744.
27. N. Kitazawa, Y. Watanabe, Y. Nakamura, *Journal of Materials Science.* **2002,** *37*, 3585-3587.
28. N. Droseros, G. Longo, J. Brauer, M. Sessolo, H. Bolink, N. Banerji. *ACS Energy Letters.* **2018,** *3*, 1458-1466.
29. G. Müller, A. Friedberger, K. Knese, in *Handbook of Silicon Based MEMS Materials and Technologies* (Eds.: V. Lindroos, M. Tilli, A. Lehto, T. Motooka), William Andrew Publishing, Boston, **2010**, pp. 409-431.
30. P. Schulz, E. Edri, S. Kirmayer, G. Hodes, D. Cahen, A. Kahn, *Energy & Environmental Science* **2014**, *7*, 1377-1381.
31. M. Byranvand, A. Kharat, N. Taghavinia. *Materials Letters.* **2019,** *237*, 356-360.
32. Z. Xiao, Y. Yuan, Y. Shao, Q. Wang, Q. Dong, C. Bi, P. Sharma, A. Gruverman, J. Huang. *Nature Materials.* **2014,** *14*, 193.
33. R. Misra, S. Aharon, B. Li, D. Mogilyansky, I. Visoly-Fisher, L. Etgar, E. Katz. *The Journal of Physical Chemistry Letters.* **2015,** *6* (3), 326-330.
34. J. Pan, S. P. Sarmah, B. Murali, I. Dursun, W. Peng, M. R. Parida, J. Liu, L. Sinatra, N. Alyami, C. Zhao, E. Alarousu, T. K. Ng, B. S. Ooi, O. M. Bakr, O. F. Mohammed, *The Journal of Physical Chemistry Letters* **2015**, *6*, 5027-5033.
35. A. Loiudice, S. Saris, E. Oveisi, D. Alexander, R. Buonsanti. *Angewandte Chemie International Edition.* **2017,** *56* (36), 10696-10701.
36. J. Burschka, N. Pellet, S.-J. Moon, R. Humphry-Baker, P. Gao, M. Nazeeruddin, M. Grätzel. *Nature* **2013,** *499*, 316.
37. K. Lim, C. Deakin, B. Ding, X. Bai, P. Griffin, T. Zhu, R. Oliver, D. Credgington, *APL Materials.* **2019,** *7* (2), 021107.
38. D. Dirin, L. Protesescu, D. Trummer, I. Kochetygov, S. Yakunin, F. Krumeich, N. Stadie, M. Kovalenko. *Nano Letters.* **2016,** *16* (9), 5866-5874.
39. R. Gonzalez-Rodriguez, N. Arad-Vosk, A. Sa'ar, J. Coffer. *The Journal of Physical Chemistry C.* **2018,** *122* (34), 20040-20045.
40. N. Arad-Vosk, N. Rozenfeld, R. Gonzalez-Rodriguez, J. Coffer, A. Sa'ar. *Phys. Rev. B.* **2017**, *95*,085433
41. R. Gonzalez-Rodriguez, N. Arad-Vosk, N. Rozenfeld, A. Sa'ar, J. Coffer. *Small.* **2016**, *12*, 4477–4480.
42. X. Huang, R. Gonzalez-Rodriguez, R. Rich, Z. Gryczynski, J. Coffer. *Chemical Communications.* **2013,** *49* (51), 5760-5762.
43. V. Malgras, S. Tominaka, J. Ryan, J. Henzie, T. Takei, K. Ohara, Y. Yamauchi. *Journal of the American Chemical Society.* **2016,** *138* (42), 13874-13881
44. R. Nemanich, D. Biegelsen, R. Street, B. Downs, B. Krusor, R. Yingling. (H.K. Choi, R. Hull, H. Ishiware and R.J. Nemanich, eds). *Pittsburgh: Materials Research Society,* **1988,** *116,* 245-250.
45. V. Malgras, J. Henzie, T. Takei, Y. Yamauchi. *Chemical Communications.* **2017,** *53* (15), 2359-2362.
46. S. Leyre, E. Coutino-Gonzalez, J. J. Joos, J. Ryckaert, Y. Meuret, D. Poelman, P. F. Smet, G. Durinck, J. Hofkens, G. Deconinck, and P. Hanselaer, *Rev. Sci. Instr.,***2014**, 85, 123115.
47. R. Brenes, D. Guo, A. Osherov, N. K. Noel, C. Eames, E. M. Hutter, S. K. Pathak, F. Niroui, R. H. Friend, M. S. Islam, H. J. Snaith, V. Bulović, T. J. Savenije, S. D. Stranks, *Joule* **2017**, *1*, 155-167.
48. M. Anaya, J. F. Galisteo-López, M. E. Calvo, J. P. Espinós, H. Míguez, *The Journal of Physical Chemistry Letters* **2018**, *9*, 3891-3896.
49. R. Brenes, C. Eames, V. Bulović, M. S. Islam, S. D. Stranks, *Advanced Materials* **2018**, *30*, 1706208.
50. Y. Tian, M. Peter, E. Unger, M. Abdellah, K. Zheng, T. Pullerits, A. Yartsev, V. Sundström, I. G. Scheblykin, *Physical Chemistry Chemical Physics* **2015**, *17*, 24978-24987.

51. C. de Weerd, L. Gomez, H. Zhang, W. J. Buma, G. Nedelcu, M. V. Kovalenko, T. Gregorkiewicz, *The Journal of Physical Chemistry C* **2016**, *120*, 13310-13315.
52. J. Kim, R. Godin, S. D. Dimitrov, T. Du, D. Bryant, M. A. McLachlan, J. R. Durrant, *Advanced Energy Materials* **2018**, *8*, 1802474.
53. N, Turro, *Modern Molecular Photochemistry, New York: Benjamin Cummings.* **1978**, 317-319.
54. I. Mihalcescu, J. C. Vial, A. Bsiesy, F. Muller, R. Romestain, E. Martin, C. Delerue, M. Lannoo, and G. Allan, *Phys. Rev. B* **1995**, 51, 17605
55. J. M. Richter, M. Abdi-Jalebi, A. Sadhanala, M. Tabachnyk, J. P. H. Rivett, L. M. Pazos-Outón, K. C. Gödel, M. Price, F. Deschler, R. H. Friend, *Nature Communications* **2016**, *7*, 13941.